Early View

Original Research Article

A novel SPECT-CT imaging platform for quantifying in vivo lung cytokine signals in COPD

Benjamin Welham, Michael Bennett, Kristoffer Ostridge, Matthew Guy, Clint Zvavamwe, Anna Chilcott, Sandra Johns, Francis Sundram, Cosma M. Spalluto, Emily Shaw, Stephen Harden, Aiman Alzetani, Paul Lee, Matthew Lawson, Peter Lackie, Sofia Michopoulou, Darren Henley, Alex Kong, Aishath Fazleen, Doriana Cellura, Christopher McCrae, Adam Platt, Maria G. Belvisi, Karl J. Staples, Tom Wilkinson

Please cite this article as: Welham B, Bennett M, Ostridge K, *et al.* A novel SPECT-CT imaging platform for quantifying *in vivo* lung cytokine signals in COPD. *ERJ Open Res* 2025; in press (https://doi.org/10.1183/23120541.01246-2024).

This manuscript has recently been accepted for publication in the *ERJ Open Research*. It is published here in its accepted form prior to copyediting and typesetting by our production team. After these production processes are complete and the authors have approved the resulting proofs, the article will move to the latest issue of the ERJOR online.

Copyright ©The authors 2025. This version is distributed under the terms of the Creative Commons Attribution Non-Commercial Licence 4.0. For commercial reproduction rights and permissions contact permissions@ersnet.org

A novel SPECT-CT imaging platform for quantifying in vivo lung cytokine signals in COPD

Authors: Benjamin Welham^{1,2*}, Michael Bennett^{1,2}, Kristoffer Ostridge^{2,3}, Matthew Guy⁴, Clint Zvavamwe⁵, Anna Chilcott⁴, Sandra Johns⁴, Francis Sundram⁴, Cosma M. Spalluto², Emily Shaw², Stephen Harden^{1,6}, Aiman Alzetani^{1,2}, Paul Lee¹, Matthew Lawson², Peter Lackie², Sofia Michopoulou⁴, Darren Henley⁵, Alex Kong^{1,2}, Aishath Fazleen^{1,2}, Doriana Cellura², Christopher McCrae⁷, Adam Platt⁸, Maria G. Belvisi^{9,10}, Karl J. Staples^{1,2}, Tom Wilkinson^{1,2}

Affiliations:

¹ Southampton NIHR Respiratory Biomedical Research Centre, University Hospital Southampton; Southampton, UK.

² Clinical and Experimental Sciences, Faculty of Medicine, University of Southampton; Southampton, UK.

³ Translational Science and Experimental Medicine, Research and Early development, Respiratory and Immunology R&D BioPharmaceuticals, Astrazeneca; Gothenburg, Sweden.

⁴ Nuclear Medicine, Nuclear Medicine Physics & Radiopharmacy, University Hospital Southampton; Southampton, UK.

⁵ Radiopharmacy Department, Nuclear Medicine Physics & Radiopharmacy, University Hospital Southampton; Southampton, UK.

⁶ Department of Radiology, University Hospital Southampton; Southampton, UK.

⁷ Translational Science and Experimental Medicine, Research and Early Development, Respiratory & Immunology, BioPharmaceuticals R&D, AstraZeneca; Gaithersburg, USA

⁸ Translational Science and Experimental Medicine, Research and Early Development, Respiratory & Immunology, BioPharmaceuticals R&D, AstraZeneca; Cambridge, UK.

⁹ Research and Early Development, Respiratory & Immunology, BioPharmaceuticals R&D, AstraZeneca; Gothenburg, Sweden.

¹⁰ National Heart and Lung Institute, Imperial College; London, UK

* Corresponding author

Correspondence email: b.welham@soton.ac.uk

Keywords: Molecular imaging, inflammation, SPECT-CT, COPD, automated

Take home message:

Disease modifying treatments in COPD are currently lacking. Our novel platform for imaging inflammatory cytokine activity in airways disease may provide a new precision medicine approach to determine the most appropriate treatment for an individual

Abstract:

Introduction:

Disease-modifying treatments such as monoclonal antibodies can be highly effective in chronic inflammatory diseases such as COPD, but often fail in clinical trials due to heterogeneity of inflammation and imperfect tools to stratify patients to select optimal therapeutic approaches. Molecular imaging provides the potential to transform precision medicine in this field.

Methods:

We developed and tested a novel molecular imaging platform using therapeutic monoclonal antibodies labelled with SPECT-CT detectable markers to quantify *in vivo* TNF involved in chronic lung inflammation in humans. We undertook a proof-of-concept clinical study involving participants with COPD and healthy controls. Participants underwent SPECT-CT imaging at 6- and 24-hours following injection of ^{99m}Tc-anti-TNF. Segmentation of lung regions and ^{99m}Tc-anti-TNF activity quantification was undertaken using novel semi-automated and AI-driven approaches.

Results:

A significant increase in normalised activity, representing increased TNF inflammatory activity, was seen between the two time-points in the COPD group (64.88% +/- [SD] 31.04, p=.029) and not in healthy controls (35.38% +/- 34.33, p=.110). However, analysis at a single

time-point revealed higher normalised activity in the healthy group. We demonstrated that

pulmonary blood vessel density and degree of emphysema were strongly correlated with this

activity signal and identified as confounding factors, highlighting the need to address

differences in target-organ characteristics in COPD. Experimental methods to adjust for these

factors were developed for organ-specific signal quantification.

Conclusions:

We report novel analysis techniques for molecular imaging of the human lung, presenting a

platform which provides new insights into complex inflammatory disease and future precision

medicine approaches.

Abstract word count: 250 (limit = 250)

Main Text:

Word count (Main text without captions or tables): 3000 (limit = 3000)

INTRODUCTION

Chronic inflammation is a core process in the pathophysiology of the leading causes of

morbidity and mortality worldwide [1]. Whilst many inflammatory diseases have seen

advances in the rapeutic approaches driven by the introduction of monoclonal antibody therapy,

there remains a significant failure rate when a generic approach is taken to treating

heterogeneous inflammatory disease [2, 3]. The key translational challenge is to better

understand the mechanisms driving these conditions and to identify targets for therapy at an

individual patient level.

This challenge is perhaps most pressing in chronic obstructive pulmonary disease (COPD)

where, to date, there are no guideline-directed monoclonal therapies available. Extrapolation

of TH2-targeted treatments developed for asthma have previously failed to consistently demonstrate effect in COPD [4–7]. Biomarker-driven strategies which rely on peripheral blood markers such as the eosinophil count and total IgE have shown benefit in directing asthma biologic treatment [8–10] and recent emerging evidence suggests this to also be the case for a subset of patients with COPD using anti-IL-4/IL-13 therapy [11]. However, guidelines on use and evidence of real-world efficacy are yet to be established. Furthermore, peripheral markers of inflammation do not necessarily correlate with those seen within the lung [12]. Novel precision medicine approaches to guide therapy and which directly assess markers at the site of inflammation are urgently needed.

Nuclear medicine platforms are currently under investigation to enable molecular imaging of active inflammation. Proof-of-concept studies have investigated planar scintigraphy or single photon emission computed tomography- (SPECT) computed tomography (CT) imaging following infusion of ^{99m}Tc-anti-TNF in inflammatory bowel disease, sarcoidosis and rheumatoid arthritis [13–16]. There is early evidence that this form of imaging may be of utility in developing precision medicine approaches, and significant scope to extend molecular imaging of inflammation across a broad range of disease and biological targets. However, previous hurdles interpreting imaging findings in complex and vascular organs have been noted [13, 15] and identifying SPECT gamma counts originating from tracer bound to target rather than the intravascular compartment will be challenging in emphysematous lung tissue in COPD, where there is variable loss of pulmonary vasculature [17].

We have developed an *in vivo* lung imaging platform and analytical techniques to quantify uptake of radiolabelled monoclonal antibodies in human airways disease. Tumour necrosis factor (TNF) is an inflammatory mediator in the inflammatory process of COPD [7] and has

been found to be upregulated in the sputum of patients with COPD [18]. It is hypothesised that TNF will therefore be detectable and, with appropriate innovation, quantifiable through molecular imaging. This study quantifies active inflammation *in vivo* within the lungs of patients with COPD for the first time, using SPECT-CT and novel, automated analysis approaches, as proof of principle for a new era of precision medicine in airways disease.

MATERIALS AND METHODS

Participant selection and assessments for SPECT-CT study

Study procedures were undertaken at University Hospital Southampton, United Kingdom. Five participants with severe to very-severe COPD, as defined by the Global Initiative for Chronic Obstructive Lung Disease (GOLD) [19] spirometry parameters (FEV₁ <50% predicted and FEV₁/FVC <0.70) and five never-smoker participants without any history or spirometric evidence of lung disease were recruited to the clinical study. Spirometry assessments were undertaken at enrolment. Full details of inclusion/exclusion criteria and assessments undertaken are provided in the supplementary material.

Informed consent was taken from all participants and the study procedures were undertaken in accordance with a pre-specified protocol approved by the Research Ethics Committee (reference 18/SC/0359) and Administration of Radioactive Substances Advisory Committee (ARSAC reference 357).

Radiolabelling of anti-TNF with 99mTc

Radiolabelling was undertaken by the radiopharmacy at University Hospital Southampton. Infliximab, an anti-TNF monoclonal antibody (Remicade, Janssen Biotech), was labelled with ^{99m}Tc by the direct labelling method as described previously [13, 20] (see *supplementary material*).

SPECT-CT imaging and biodistribution studies

Following collection of measurements and phenotyping data, participants underwent SPECT-CT and whole-body imaging. Prior to imaging, 370MBq radiolabelled anti-TNF (dose range 100-200 µg) was infused over 30-60 minutes in a volume of 10 mL.

Scan sequences were initiated at 6 hours (+/- 60 minutes) and 24 hours (+/- 4 hours) following start of infusion. Imaging was obtained using a Symbia Intevo Bold (Siemens Healthcare GmbH, Germany) 16-slice double headed gamma camera system. All participants underwent whole-body planar imaging, SPECT imaging of the chest and low-dose CT (LDCT) of the thorax at each time-point. Participants in the COPD group had an additional high-resolution CT (HRCT) of the thorax at the 6-hour time-point. The first participant in each group also underwent whole body planar imaging at 3 hours (+/-30minutes) following infusion for additional dosimetry calculations (see *supplementary material* for full scan protocol details).

Image processing and analysis

The CT data was initially analysed and segmented using Southampton Pulmonary Radiomics software (version beta-e3b7ef8254). A region of interest (RoI) including both lung volumes was defined through this process and SPECT activity normalised to account for differing biological clearance between participants. Details of the segmentation, SPECT registration and normalisation process are included in the supplementary material.

To determine binding of the monoclonal antibody to target, the percentage change in normalised counts between the 6- and 24-hour scans was calculated. This measure has previously been used in studies imaging inflammation in other disease groups and correlates with disease markers and likelihood of response to therapy. A greater increase in activity at the later scan time-point, when more of the activity has cleared from the blood circulation, represents greater tissue cytokine activity [14, 16]. Activity at each time point was also quantified individually.

Unbound antibody within the blood compartment flows through the RoI and does not represent the presence of TNF in tissue. Furthermore, it was hypothesised that antibody deposition would be decreased in emphysematous regions due to loss of tissue density. We therefore undertook an analysis of these potential confounding factors using automated approaches. Emphysema was quantified by percentage of voxels with low attenuation area <-950 Hounsfield units (%LAA.950). Blood vessels were segmented using an AI-driven approach developed through creation of a labelled training dataset. This data was used to develop an experimental calculation to correct for the presence of emphysema and to subtract activity contained within

blood vessels. A full description of the image analysis methods is provided in the supplementary material.

Immunohistochemistry studies

To determine localization of TNF in lung tissue to inform the clinical study, an immunohistochemistry study was undertaken on previously collected lung tissue samples separate to the clinical imaging study cohort. Samples for immunohistochemistry studies were obtained from the TargetLung (REC number 14/SC/0186) study. Details are provided in the supplementary material.

Statistical analysis

Median normalised counts (C_n) were used as the summary statistic for each patient as voxel counts across the lung volume were non-normally distributed (*figure 1*). Group statistics are calculated as mean of these summary statistics. Student's t-test was used for between group comparisons, paired t-test for comparisons between two time-points in the same group, and Spearman's correlation coefficient for correlations between C_n and other factors. Between group differences in vessel density and age range were analysed by Mann-Whitney U test. A multiple linear regression model was applied to determine the combined effects of the two main confounding factors, as well as participant group, on SPECT activity. Data was analysed with SPSS statistics 27 software (IBM, United States) and voxel-wise data was analysed in Matlab (The MathWorks Inc, United States).

RESULTS

Study population

Five participants were recruited with severe to very-severe COPD according to GOLD classification (group mean [+/- standard deviation] post-bronchodilator FEV1 %predicted 32.80 +/- 9.83), and five never smoker participants without any underlying lung disease. Mean age +/-SD in the COPD group was 72.0 (+/-9.23) and 66.2 (+/-2.35) in the control group. Participants were selected to ensure no statistically significant age difference between groups (p=0.151). Details of participant characteristics and spirometry results are shown in *table 1*.

Evidence of increased 99mTc-anti-TNF binding in patients with COPD

The increase in C_n between the 6- and 24-hour time-point was significant only in the COPD group (p=0.029, *figure 1*) suggesting greater pulmonary tissue TNF levels in this group. C_n increased by a mean of 35.38% +/- 34.33 in the healthy group and 64.88% +/- 31.04 in the COPD group. As TNF is a pro-inflammatory cytokine known to be upregulated in COPD [18], the results suggest that TNF is detectable using this approach.

99mTc-anti-TNF quantification is influenced by key disease relevant confounding factors

We also examined C_n at each scan time-point individually. Conversely to the change over time, analysis of C_n between groups demonstrated that it was higher in the healthy group than in COPD at both time-points. Within the healthy group, mean of the patient-wise summary statistics was 0.182 ± 0.027 and 0.087 ± 0.019 in the COPD group at the 6-hour time-point. At the 24-hour time-point, mean of the summary statistics for the healthy group was 0.250 ± 0.089 and 0.147 ± 0.056 for the COPD group (*figure 1*). The difference between groups was only statistically significant at 6-hours (p<0.001).

Reasons for the higher signal at individual time-points in the healthy group were examined to create a disease-relevant quantitative model. COPD is known to be associated with heterogenous structural changes to tissue which could confound quantification of antibody binding. Our immunohistochemistry work confirmed TNF expression within the alveolar and airway epithelium (*figure 2*, **A**), which is lost as emphysema develops in advanced COPD. Additionally, there will be patient-to-patient differences in amount of unbound tracer circulating through pulmonary blood vessels as pulmonary vasculature is known to be lost in COPD [17]. We examined the effect of each of these factors on ^{99m}Tc-anti-TNF uptake.

Mean vessel density in the healthy group was 0.132 ± 0.023 and was 0.088 ± 0.018 in the COPD group. The differences between groups were statistically significant (p=0.016). When vessel density was plotted against C_n , a clear positive correlation emerged at both time-points (figure 2). Spearman's r at the 6-hour time-point was 0.794 (p=0.006) and 0.745 (p=0.013) at the 24-hour time-point. This finding suggests that quantification of activity is affected by vessel loss in COPD [17].

A clear negative correlation was seen between C_n and CT-detected emphysema using the established density mask %LAA₋₉₅₀ (*figure 2*). At the 6-hour time-point, Spearman's r was - .700 (p=0.188) and at the 24-hour time-point was -1.000 (p<0.01). This association was also visible qualitatively on scan slices as shown in *figure 3* and confirms the confounding effect of COPD-related tissue changes on antibody binding levels due to tissue loss.

Adjusting for tissue heterogeneity

Application of a correction algorithm to subtract the ^{99m}Tc-anti-TNF signal contained within the pulmonary vasculature revealed mean of the corrected normalised counts within the healthy volunteer group at the 6-hour time-point of 0.051 +/- 0.031 and -0.001 +/- 0.007 in the COPD group (p=0.007). At the 24-hour time-point, the mean of the corrected normalised counts in the healthy group was 0.118 +/- 0.073 and in the COPD group was 0.058 +/- 0.044 (p=.155, *figure* 4, **B** and **C**). The negative value at the 6-hour time-point suggests over-correction by this method, and the trend of higher counts within the healthy group compared to the COPD group remained.

An alternative correction was tested to adjust for the effect of tissue density loss due to emphysema. Assuming %LAA₋₉₅₀ of zero in the healthy group, at the 6-hour time-point corrected counts were (mean +/- SD) 0.182 +/- 0.027 in the healthy group and 0.225 +/- 0.038 in the COPD group (*figure 4*, **A**). At the 24-hour time-point this was 0.250 +/- 0.089 in the healthy group and 0.285 +/- 0.017 in the COPD group. A further conservative analysis assuming %LAA₋₉₅₀ in healthy subjects of 2% did not reverse this trend of higher corrected

counts in the COPD group (see *supplementary material*). Differences between groups were not statistically significant in either analysis.

Discussion

Our results outline a novel approach to imaging in COPD, using automated analysis techniques to quantitatively analyse target cytokine levels in lung tissue. By identifying patients as having high or low levels of target cytokines present, we aim to more effectively stratify whether patients are suitable for treatments targeting these pathways. To develop and test the imaging platform, we imaged TNF activity as this is a cytokine known to be involved in chronic inflammation in COPD [18]. In addition, infliximab is a licensed therapeutic monoclonal antibody which binds both soluble and transmembrane TNF [21], has previously been labelled with technetium-99m and has proven safety and utility for molecular imaging of inflammation in other disease groups using alternative imaging methodology [13, 14, 16]. It is therefore an ideal tool molecule for platform development.

Differences between disease and control groups were clearly defined using the change in detected C_n between the 6- and 24-hour time-point scans. This reflects findings in prior literature and is of importance as the difference in uptake between two scan time-points is a measure for which there is prior early evidence of ability to select those more likely to respond to specific therapies [14, 16].

Molecular imaging of inflammation in complex organs such as the lungs presents additional challenges due to heterogeneity of tissue structure. Using the change in activity between 6- and 24-hour scans may account for between-participant heterogeneity. If analysing data at a single time-point, which is optimal in a clinical setting, structural heterogeneity needs to be

considered, especially in the COPD population. A fall in vessel density and a rise in the degree of emphysema are known features for these patients [17].

Analysis of these confounding factors indicated that SPECT activity originating from blood vessels flowing through the RoI contributed to normalised activity and varied between patients. To determine target cytokine activity, only the distribution of antibody bound to its target is relevant, so we developed methods to subtract signal from unbound antibody flowing through vasculature. Evidence of over-correction was seen at the 24-hour time-point, possibly in part due to partial-volume effects of LDCT resulting in the volume of vessels being exaggerated, as well as movement artefact during free-breathing scans. Breath-hold, HRCT scans could overcome these obstacles, but at the expense of higher radiation dose to participants. Other examples of correction approaches include those previously tested in Positron Emission Tomography (PET)-CT imaging, where correction approaches have used Hounsfield unit values and kinetics models to determine how standard uptake values (SUV) are affected by the fraction of voxels occupied by tissue, air or blood [22].

Loss of lung tissue density due to emphysema was also negatively correlated with detected signal. The immunohistochemistry results show that TNF is expressed within tissue compartments which are lost in the development of emphysema, such as alveolar and airway epithelium. Loss of pulmonary vasculature is also associated with the development of emphysema [17], therefore emphysema is likely a composite factor accounting for the loss of detected 99m Tc-anti-TNF signal. Correction for emphysema provided a return to the expected trend of higher signal in the COPD group. Lack of statistical significance may be in part due to the small sample size. A multiple regression model (see *supplementary material*) accounting for both confounding factors simultaneously also indicated that expected C_n at the 24-hour

time-point after adjustment for both emphysema and vessel density was higher in the COPD group, but this result was not statistically significant. An expanded dataset to more accurately determine the effects of tissue and vessel density on C_n may provide improved performance of any corrections undertaken, as the small sample size limits generalisability. Studies involving repeat imaging on the same participants may also help determine reproducibility, but are limited by the additional radiation exposure this entails. Furthermore, imaging in early disease, where lung tissue is less heterogenous, may eliminate any need for tissue density corrections.

Other analysis methods used for PET-CT imaging protocols may be applicable for similar future studies. Maximum standardised uptake value (SUV_{max}) is a measure commonly used in PET imaging [23]. Whilst this is of use in oncological applications investigating tumour sources, it is likely that SUV_{max} voxels in our study would correspond to regions of vasculature. Another approach, similar to the analysis of difference between 6- and 24-hour data in our study, is dynamic PET and kinetic modelling which involves more complex modelling of the movement of tracer over time into areas of target activity [24].

It should be noted that the physical half-life of SPECT isotopes should ideally match the biological half-life of the antibody used. The half-life of ^{99m}Tc at 6.02 hours is significantly shorter than that of monoclonal antibodies, which have biological half-lives of many days. Tracers with longer half-lives such as ¹²³I could provide utility beyond 24 hours when antibody binding may be more specific, but at the expense of higher radiation dose [25]. Suitable PET tracers also generally involve greater radiation dose to participants and some degradation of image quality, especially in heterogenous and low-density tissue, due to increased positron range [26].

Previous studies have investigated the use of molecular imaging approaches to determine target cytokine activity or predict response to therapy in other inflammatory diseases including rheumatoid arthritis, Crohn's disease and sarcoidosis [13, 14, 16]. No platforms or analysis techniques exist which are approved for clinical use. Our data reveals that it is possible to image and non-invasively quantify inflammatory cytokine activity *in vivo* in complex organs such as the lung, providing a window into the active inflammatory process at the site of disease activity for an individual.

We provide proof-of-concept for molecular imaging of inflammation in airways disease for the first time, using novel semi-automated analysis techniques to determine whole-organ regions of interest, whilst accounting for patient-specific heterogeneity of tissue. Further development and investigation in larger scale clinical trials is needed to fully define its utility as a non-invasive imaging biomarker. Future work imaging clinically relevant inflammatory pathways such as TH2-driven inflammation would also be of value, allowing comparison of imaging biomarkers with established blood biomarkers of disease activity. Identification of the correct therapy for a patient without the need for lengthy treatment trials of ineffective therapy may be attainable using approaches such as this for a future of molecular imaging-driven precision medicine.

ACKNOWLEDGEMENTS

We would like to thank Dr Serena Chee (University Hospital Southampton), Benjamin Johnson and Lydia Scarlett (TargetLung Clinical Trials Associates) for their oversight and assistance in collection of lung specimens as part of the TargetLung study. Also, Dr Jon Ward, Jenny Norman and Monette Lopez (Histochemistry Research Unit, University of Southampton) for their work providing sections and assistance with TNF immunohistochemistry. We would also like to thank Bethany Armstead, Esther Nyimbili, Marta Cabral and Glenda Jones for their support delivering the clinical element of the study. Thanks also to Dr Konstantina Iliadi, Dr Neil O'Brien and Dr Tim Melhuish for their input in image analysis and medical physics support, Professor Stephen Mather for his advice and support regarding radiopharmaceutical labelling, as well as Dr Hang Phan for her statistical advice.

	Control (n= 5)	COPD (<i>n</i> = 5)
Characteristics Age, mean (SD)	66.20 (9.23)	72.00 (2.35)
Gender, Female	2	2
Smoking status, Never / ex / current	5 / 0 / 0	0 / 3 / 2
Smoking history, mean pack years (SD)	0 (0)	41.60 (6.11)
FEV1 % predicted pre-bronchodilator, mean (SD)	114.60 (10.92)	29.80 (10.99)
FVC % predicted pre-bronchodilator, mean (SD)	121.40 (13.72)	71.00 (5.61)
FEV1/FVC pre-bronchodilator, mean (SD)	0.736 (0.056)	0.316 (0.102)
FEV1 % predicted post-bronchodilator, mean (SD)	118.80 (12.99)	32.80 (9.83)
FVC % predicted post-bronchodilator, mean (SD)	121.20 (15.12)	75.00 (6.75)
FEV1/FVC post-bronchodilator, mean (SD)	0.762 (0.058)	0.346 (0.093)
TLCO % predicted, mean (SD)	105.00 (21.48)	49.20 (11.23)
RV % predicted, mean (SD)	92.60 (18.98)	180.60 (42.19)
RV/TLC, mean (SD)	0.334 (0.067)	0.628 (0.072)
CAT score, mean (SD)	3.00 (1.73)	20.80 (4.66)
mMRC score, mean (SD)	0 (0)	2.40 (0.55)

Table 1. Characteristics of recruited participants at baseline for the clinical imaging study. This includes age, gender, smoking status, pulmonary function test results and questionnaire results. FEV1, forced expiratory volume in 1 second; FVC, forced vital capacity; TLCO, transfer factor of the lung for carbon monoxide; RV, residual volume; TLC, total lung capacity; CAT, COPD assessment tool; mMRC, modified Medical Research Council dyspnoea scale.

REFERENCES:

- The top 10 causes of death [Internet]. World Health Organisation 2020 [cited 2021 Mar 16]. Available from: https://www.who.int/news-room/fact-sheets/detail/the-top-10-causes-of-death.
- Bek S, Bojesen AB, Nielsen J V., *et al.* Systematic review and meta-Analysis: Pharmacogenetics of anti-TNF treatment response in rheumatoid arthritis. *Pharmacogenomics Journal* [Internet] Nature Publishing Group; 2017; 17: 403–411. Available from: http://dx.doi.org/10.1038/tpj.2017.26.
- 3 Côté-Daigneault J, Bouin M, Lahaie R, *et al.* Biologics in inflammatory bowel disease: what are the data? *United European Gastroenterol J* 2015; 3: 419–428.
- 4 Criner GJ, Celli BR, Brightling CE, *et al.* Benralizumab for the prevention of COPD exacerbations. *New England Journal of Medicine* 2019; 381: 1023–1034.
- Pavord ID, Chanez P, Criner GJ, et al. Mepolizumab for eosinophilic chronic obstructive pulmonary disease. New England Journal of Medicine 2017; 377: 1613–1629.
- Rennard SI, Fogarty C, Kelsen S, *et al.* The safety and efficacy of infliximab in moderate to severe chronic obstructive pulmonary disease. *Am J Respir Crit Care Med* 2007; 175: 926–934.
- Prightling C, Greening N. Airway inflammation in COPD: Progress to precision medicine. *European Respiratory Journal* [Internet] 2019; 54. Available from: http://dx.doi.org/10.1183/13993003.00651-2019.
- Humbert M, Beasley R, Ayres J, *et al.* Benefits of omalizumab as add-on therapy in patients with severe persistent asthma who are inadequately controlled despite best available therapy (GINA 2002 step 4 treatment): INNOVATE. *Allergy: European Journal of Allergy and Clinical Immunology* 2005; 60: 309–316.
- Ortega HG, Liu MC, Pavord ID, *et al.* Mepolizumab treatment in patients with severe eosinophilic asthma. *New England Journal of Medicine* 2014; 371: 1198–1207.
- Bleecker ER, FitzGerald JM, Chanez P, *et al.* Efficacy and safety of benralizumab for patients with severe asthma uncontrolled with high-dosage inhaled corticosteroids and long-acting β2-agonists (SIROCCO): a randomised, multicentre, placebo-controlled phase 3 trial. *The Lancet* 2016; 388: 2115–2127
- Bhatt SP, Rabe KF, Hanania NA, *et al.* Dupilumab for COPD with Type 2 Inflammation Indicated by Eosinophil Counts. *New England Journal of Medicine* Massachusetts Medical Society; 2023; .
- 12 Schleich FN, Chevremont A, Paulus V, *et al.* Importance of concomitant local and systemic eosinophilia in uncontrolled asthma. *European Respiratory Journal* European Respiratory Society; 2014; 44: 97–108
- D'Alessandria C, Malviya G, Viscido A, *et al.* Use of a 99mTc labeled anti-TNFa monoclonal antibody in Crohn's disease: in vitro and in vivo studies. *The Quarterly Journal of Nuclear Medicine and Molecular Imaging* 2007; : 334–342.
- 14 Conti F, Malviya G, Ceccarelli F, *et al.* Role of scintigraphy with 99mTc-infliximab in predicting the response of intraarticular infliximab treatment in patients with refractory monoarthritis. *Eur J Nucl Med Mol Imaging* 2012; 39: 1339–1347.
- Galli F, Lanzolla T, Pietrangeli V, *et al.* In vivo evaluation of TNF-alpha in the lungs of patients affected by sarcoidosis. *Biomed Res Int* 2015; 2015.
- Vis R, Malviya G, Signore A, *et al.* 99mTc-anti-TNF-α antibody for the imaging of disease activity in pulmonary sarcoidosis. *European Respiratory Journal* [Internet] 2016; 47: 1198–1207. Available from: http://dx.doi.org/10.1183/13993003.01352-2015.
- Estépar RSJ, Kinney GL, Black-Shinn JL, *et al.* Computed Tomographic Measures of Pulmonary Vascular Morphology in Smokers and Their Clinical Implications. *Am J Respir Crit Care Med* [Internet] 2013; 188: 231–239. Available from: https://www.atsjournals.org/doi/10.1164/rccm.201301-0162OC.
- 18 Keatings VM, Collins PD, Scott DM, *et al.* Differences in interleukin-8 and tumor necrosis factor-alpha in induced sputum from patients with chronic obstructive pulmonary disease or asthma. *Am J Respir Crit Care Med* [Internet] 1996; 153: 530–534. Available from: http://www.atsjournals.org/doi/abs/10.1164/ajrccm.153.2.8564092.
- 19 COPD Global Initiative. GOLD 2020 Report. *Global Initiative for Chronic Obstructive Lung Disease* 2020; .
- Mather SJ, Ellison D. Reduction-mediated technetium-99m labeling of monoclonal antibodies. *Journal of Nuclear Medicine* 1990; 31: 692–697.
- Kaymakcalan Z, Sakorafas P, Bose S, *et al.* Comparisons of affinities, avidities, and complement activation of adalimumab, infliximab, and etanercept in binding to soluble and membrane tumor necrosis factor. *Clinical Immunology* 2009; 131: 308–316.

- Holman BF, Cuplov V, Millner L, *et al.* Improved correction for the tissue fraction effect in lung PET/CT imaging. *Phys Med Biol* [Internet] IOP Publishing; 2015; 60: 7387–7402. Available from: http://dx.doi.org/10.1088/0031-9155/60/18/7387.
- Graham MM. Quantification of Radiotracer Uptake Into Tissue. *Molecular Imaging: Principles and Practice* Elsevier; 2021. p. 1613–1624.
- Dimitrakopoulou-Strauss A, Pan L, Sachpekidis C. Kinetic modeling and parametric imaging with dynamic PET for oncological applications: general considerations, current clinical applications, and future perspectives. Available from: https://doi.org/10.1007/s00259-020-04843-6.
- McCarthy CE, White JM, Viola NT, *et al.* In vivo Imaging Technologies to Monitor the Immune System. *Front Immunol* 2020; 11: 1–21.
- Emond EC, Groves AM, Hutton BF, *et al.* Effect of positron range on PET quantification in diseased and normal lungs. *Phys Med Biol* Institute of Physics Publishing; 2019; 64.

STATEMENTS AND DECLARATIONS:

Declaration of interests

Tom Wilkinson has received grant funding and/or consultancy fees from: AstraZeneca, GlaxoSmithKline, Boehringer Ingelheim, Teva Pharmaceuticals, Synairgen, Bergenbio, Union Chimique Belge, Sanofi and Epiendo pharmaceuticals. Tom Wilkinson is founder and Director of mymhealth. Tom Wilkinson and Michael Bennett are founders of an imaging spin-out company, Precision Clinical Intelligence. Tom Wilkinson, Michael Bennett and Benjamin Welham are listed as inventors on a submitted patent UK patent application number GB2213773.1 – 'Apparatus and method for monitoring disease'. Kristoffer Ostridge, Maria Belvisi, Christopher McCrae and Adam Platt are employees of AstraZeneca. All other authors have no conflicts of interest to declare.

Funding

Funding was received from Astrazeneca to undertake the study.

Author contributions

Authors Kristoffer Ostridge, Tom Wilkinson, Christopher McCrae, Adam Platt and Maria Belvisi contributed to the study conceptualisation. Study methodology was developed by Kristoffer Ostridge, Tom Wilkinson, Matthew Guy, Sofia Michopoulou, Benjamin Welham, Michael Bennett, Cosma Spalluto, Clint Zvavamwe, Michael Lawson, Peter Lackie, Francis Sundram, Stephen Harden, Paul Lee, Emily Shaw, Christopher McCrae, Adam Platt and Maria Belvisi. Investigation and data collection was undertaken by Benjamin Welham, Aiman Alzetani, Aishath Fazleen, Alex Kong, Francis Sundram, Stephen Harden, Sandra Johns, Doriana Cellura, Clint Zvavamwe, Darren Henley and Matthew Guy. Analysis was performed

by Benjamin Welham, Michael Bennett, Matthew Guy, Anna Chilcott, Emily Shaw, Cosma Spalluto and Karl Staples. Customised software (Southampton Pulmonary Radiomics) and code was developed by Michael Bennett. The first draft of the manuscript was written by Benjamin Welham, Michael Bennett, Anna Chilcott and Clint Zvavamwe. All authors reviewed and commented on previous versions of the manuscript. All authors read and approved the final manuscript.

LIST OF SUPPLEMENTARY MATERIALS:

1. Supplementary material document, containing figures S1-S6 and tables S1-S2

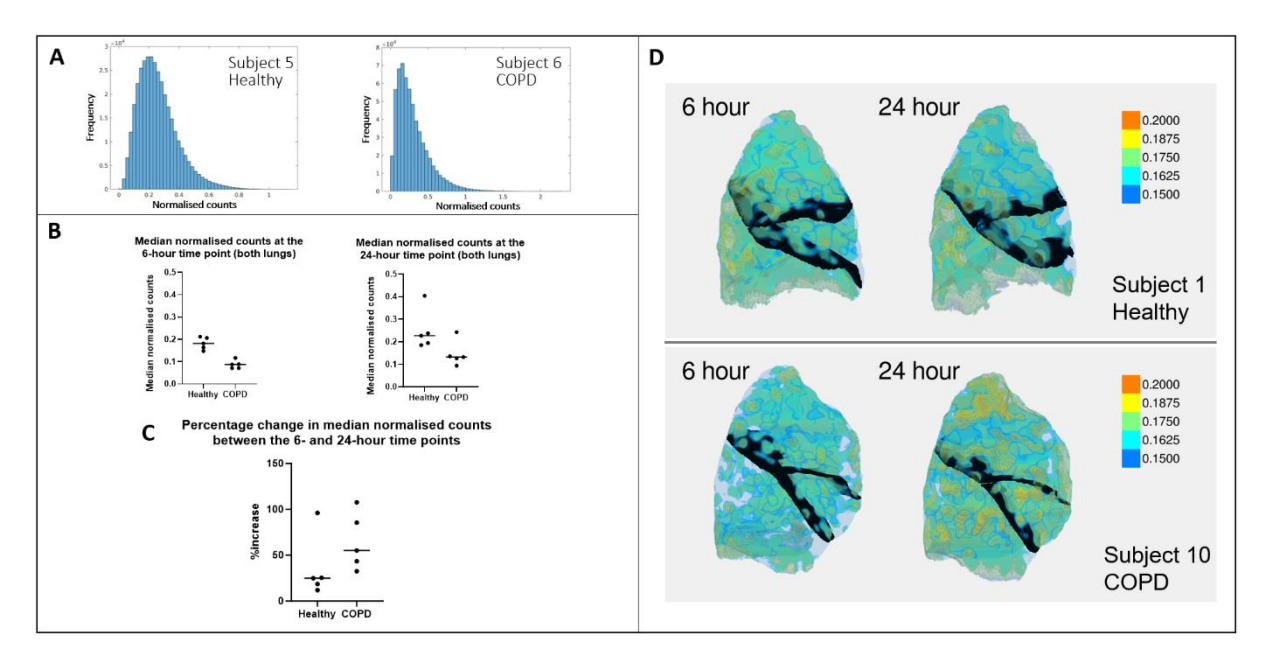


Figure 1

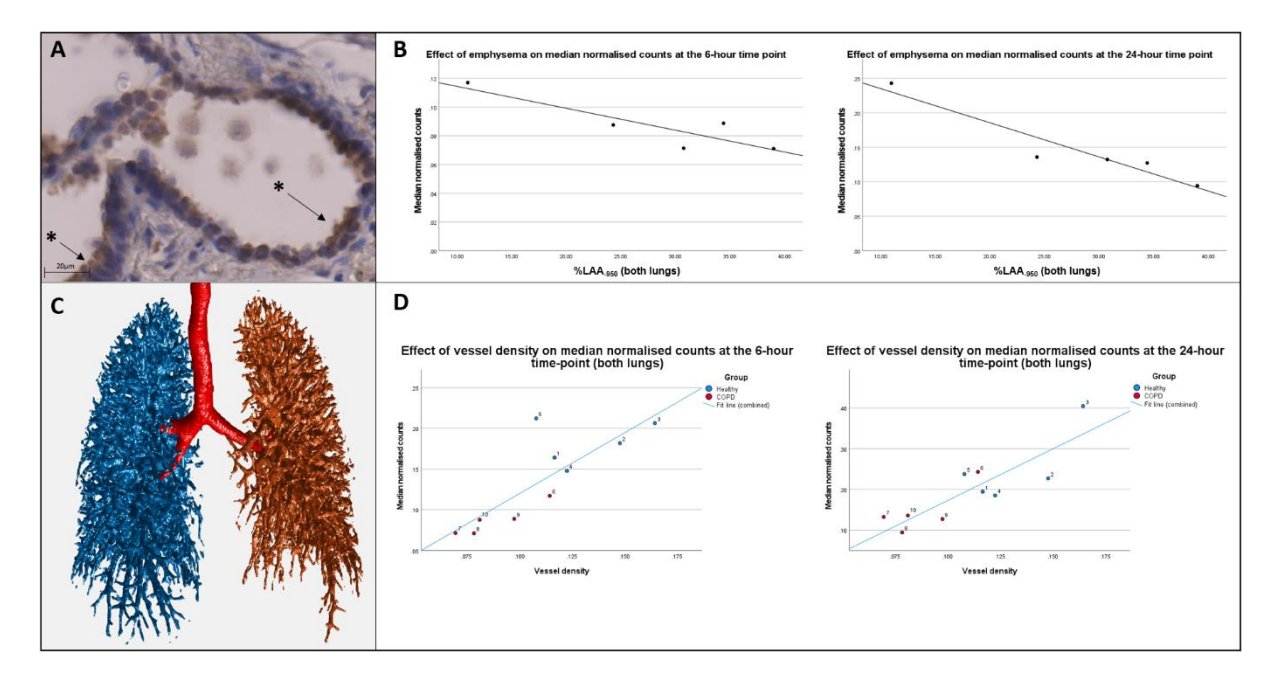


Figure 2

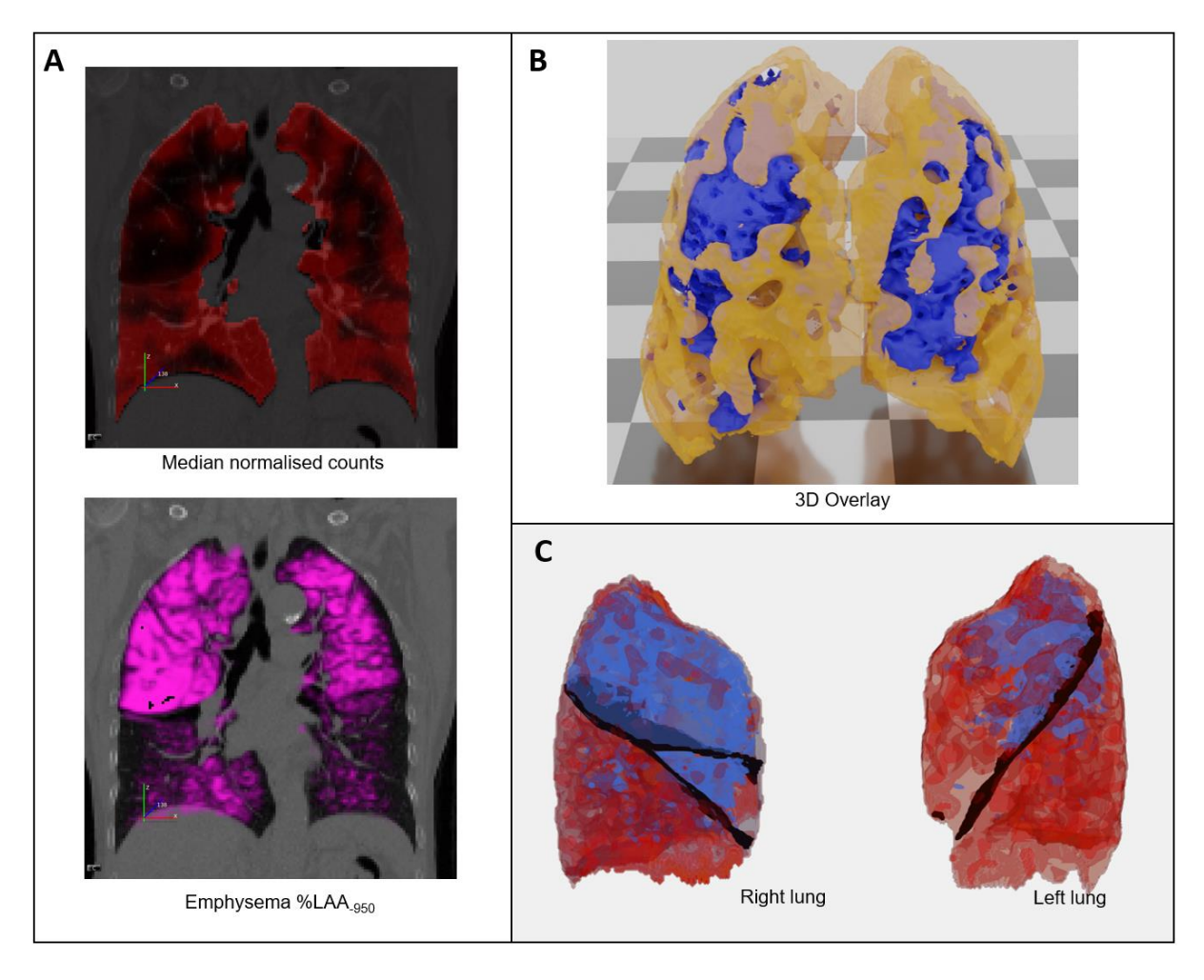


Figure 3

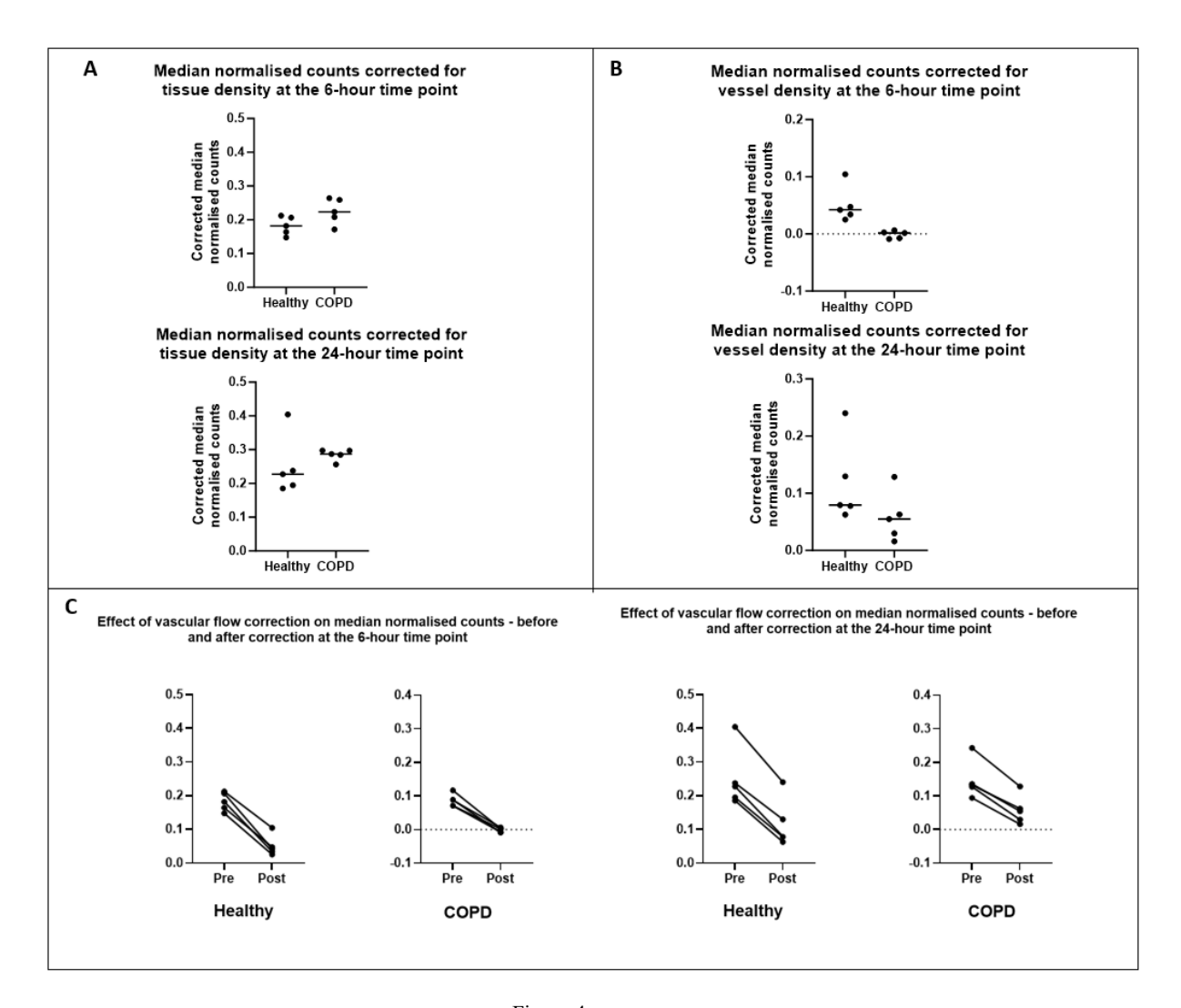


Figure 4

Supplementary material

A novel SPECT-CT imaging platform for quantifying in vivo lung cytokine signals in COPD

Authors: Benjamin Welham^{1,2*}, Michael Bennett^{1,2}, Kristoffer Ostridge^{2,3}, Matthew Guy⁴, Clint Zvavamwe⁵, Anna Chilcott⁴, Sandra Johns⁴, Francis Sundram⁴, Cosma M. Spalluto², Emily Shaw², Stephen Harden^{1,6}, Aiman Alzetani^{1,2}, Paul Lee¹, Matthew Lawson², Peter Lackie², Sofia Michopoulou⁴, Darren Henley⁵, Alex Kong^{1,2}, Aishath Fazleen^{1,2}, Doriana Cellura², Christopher McCrae⁷, Adam Platt⁸, Maria G. Belvisi^{9,10}, Karl J. Staples^{1,2}, Tom Wilkinson^{1,2}

Affiliations:

¹ Southampton NIHR Respiratory Biomedical Research Centre, University Hospital Southampton; Southampton, UK.

² Clinical and Experimental Sciences, Faculty of Medicine, University of Southampton; Southampton, UK.

³ Translational Science and Experimental Medicine, Research and Early development, Respiratory and Immunology R&D BioPharmaceuticals, Astrazeneca; Gothenburg, Sweden.

⁴ Nuclear Medicine, Nuclear Medicine Physics & Radiopharmacy, University Hospital Southampton; Southampton, UK.

⁵ Radiopharmacy Department, Nuclear Medicine Physics & Radiopharmacy, University Hospital Southampton; Southampton, UK.

⁶ Department of Radiology, University Hospital Southampton; Southampton, UK.

⁷ Translational Science and Experimental Medicine, Research and Early Development, Respiratory & Immunology, BioPharmaceuticals R&D, AstraZeneca; Gaithersburg, USA

⁸ Translational Science and Experimental Medicine, Research and Early Development, Respiratory & Immunology, BioPharmaceuticals R&D, AstraZeneca; Cambridge, UK.

⁹ Research and Early Development, Respiratory & Immunology, BioPharmaceuticals R&D, AstraZeneca; Gothenburg, Sweden.

¹⁰ National Heart and Lung Institute, Imperial College; London, UK

* Corresponding author

Correspondence email: b.welham@soton.ac.uk

Supplementary Materials and Methods

Phantom studies

Phantom studies were undertaken prior to the clinical element of the study to inform imaging

protocol design and to determine validity and limitations of the clinical imaging platform

quantitation. This allowed SPECT-CT imaging findings of a simulated participant to be compared

to a known distribution of radiation and simulated tissue density. An anthropomorphic torso

phantom containing lung, heart and liver inserts was used. The lung inserts were filled with

Styrofoam beads and water to simulate lung tissue density. Fillable Perspex spheres were placed

in the lung inserts to simulate defects. The volumes of the fillable spheres were 1, 2, 4 and 8 ml.

Different concentrations of Tc-99m were injected into the background, liver and spheres (at 22

kBq/ml, 47 kBq/ml and 92 kBq/ml respectively, decay-corrected to the scan time). A SPECT-CT

was acquired of the phantom and the images were reconstructed using the xSPECT conjugate

gradient reconstruction with 48 iterations, 1 subset, a 7mm Gaussian filter, CT-based attenuation

correction and scatter correction (figure S1). The activity concentration was measured for the four

spheres, liver and background and a recovery coefficient curve was created for the spheres.

Phantom distributions of greater complexity were also created using a radioactive InkJet printing

technique co-developed by members of the research team. Three-dimensional phantoms were

formed by transferring the required radioactive distribution to a sequence of paper sheets, each

Downloaded from https://publications.ersnet.org on July 28, 2025 by guest. Please see licensing information on first page for reuse rights.

supported in a frame representing the structural material present at each point (*figure S1*, **E**). The radioactive distribution was controlled to less than 1mm and within 10% of the intended activity concentration. The SPECT-CT protocol designed for the clinical element of the study was used to image the printed phantom and the images reviewed.

Participant selection for SPECT-CT study

Five participants with severe to very severe COPD, as per Global Initiative for Chronic Obstructive Lung Disease (GOLD) spirometry parameters, and five participants without any history of underlying lung disease were recruited to the study, undertaken at University Hospital Southampton, United Kingdom. Participants with COPD had a prior clinical diagnosis of COPD, smoking history of >10 pack years and post-bronchodilator FEV1/FVC <0.7 with FEV₁ <50% predicted. Healthy volunteers had no history of lung disease, post-bronchodilator FEV₁ >0.7 and were non-smokers defined as <1 pack-year smoking history.

Participants were excluded if they had a history of other respiratory disorders, pneumonia risk factors, chronic kidney disease (CKD) with estimated glomerular filtration rate <60 ml/min, prior lung surgery, autoimmune conditions, were taking immunosuppressant medications or other monoclonal antibodies, had a history of adverse reactions to any monoclonal antibody medication, a body mass index (BMI) outside the range 18-30, a urinary catheter in-situ or were taking any regular antibacterial, antiviral or respiratory investigational drug within the 30 days prior to enrolment visit. Subjects with COPD should not have had an exacerbation requiring treatment with oral corticosteroids within the 30 days prior to enrolment.

Phenotyping assessments and sampling

After recruitment, all participants underwent pre- and post-bronchodilator spirometry with measurement of diffusing capacity of the lungs for carbon monoxide (DLCO) and lung volumes by body plethysmography. Participants were asked to withhold their usual bronchodilator medication for 12 hours prior to this if applicable. Body measurements and bioelectrical impedance analysis was also undertaken at this visit.

Participants underwent blood sampling for safety assessments and TNF-α concentration measurements prior to imaging. Sputum induction for sampling of sputum TNF-α was also undertaken where possible and within COVID-19 infection control policy, both before and after imaging. Where blood (serum and plasma) and sputum TNF-α levels were obtained, TNF-α concentration was determined by Enzyme Linked Immunosorbent Assay (ELISA, Human TNF-α Quantikine high sensitivity ELISA, R&D Systems). Differences between groups were assessed by Mann-Whitney U test.

Radiolabelling of anti-TNF- α with ^{99m}Tc

Radiolabelling was undertaken by the radiopharmacy at University Hospital Southampton. Infliximab, an anti-TNF-α monoclonal antibody (Remicade, Janssen Biotech), was labelled with ^{99m}Tc by the direct labelling method as described previously [1, 2]. Anti-TNF-α was first reduced using excess of 2-mercaptoethanol leaving free thiol groups available for labelling with ^{99m}Tc. After 30 minutes incubation with 2-mercaptoethanol the reduced antibody was isolated and

purified using a PD-10 desalting column, based on an optical density of 280 nm using a UV spectrophotometer, and collected into cryo tubes ready for labelling with ^{99m}Tc.

A methylene diphosphate (MDP) bone-scanning kit (Draximage and Polatom) was reconstituted in 5ml of 0.9% sodium chloride to provide a solution containing 5mg medronate, 0.34mg stannous fluoride and 2mg p-aminobenzoic acid. Technetium-99m was obtained in the form of sodium pertechnetate, eluted from a ⁹⁹Mo/^{99m}Tc generator. 500 mcg of the reduced antibody was added to the solution followed by 450MBq pertechnetate to produce ^{99m}Tc-anti-TNF-α.

Determination of radiochemical purity by instant thin layer paper chromatography (ITLC) using cut and count method. ITLC is the stationary phase with 0.9% Nacl being the mobile phase. These conditions give the retention factor (Rf) value of the labelled antibody as Rf=0 and impurities Rf=1.

Image acquisition

Scan sequences were initiated at 6 hours (+/- 60 minutes) and 24 hours (+/- 4 hours) following start of infusion, as outlined in the main manuscript text. Whole body planar imaging used a 256x1024 matrix and acquisition speed of 15 cm/min at the 3-hour, 10 cm/min at the 6-hour and 5 cm/min at the 24-hour imaging time-point. SPECT imaging at 6 hours was undertaken with a 256x256 matrix, 60 views and 20 s per view. SPECT at 24 hours was undertaken with a 256x256 matrix, 60 views and 40 s per view.

SPECT imaging was performed with the patient supine and hands above head, with free-breathing LDCT imaging being obtained immediately after SPECT for all participants at both time points. The scan protocol was for tube voltage 130 kV, effective mAs 40 (with CareDOSE Automatic Exposure Control and Dose Modulation), pitch 1.0, rotation time 0.6s and reconstructed to a slice thickness of 1.5mm. Inspiratory and expiratory HRCT images were acquired at the 6-hour time point for patients with COPD only, with settings as above with the exception of effective mAs 90 (using CareDOSE) and reconstruction slice thickness of 0.75mm.

Image processing and analysis

The CT data, both HRCT and low-dose, were initially analysed using Southampton Pulmonary Radiomics (SPR) software (version beta-e3b7ef8254). Briefly, this analysis consisted of; 1) Manual identification of a seed point near the top of the trachea. 2) Automated airway segmentation followed by semi-automated editing to ensure adequate segmentation of all branches. 3) Automated segmentation of the left and right lungs. 4) Manual labelling of the airway branches, especially the right and left main bronchi. 5) Semi-automated segmentation of the lobes and fissures. 6) Automated analysis of the lobes to identify regions of emphysema based on the -950 HU threshold. 7) Segmentation of the blood vessels using a fully automated, AI-driven approach. Any further processing was performed using Matlab (version 2021a, The Mathworks Inc, Natick, MA.).

Both lungs regions were defined for each participant as the lung region of interest (RoI) through the segmentation process described above on the LDCT data. The LDCT was also used to allow the operator to manually identify the location of the aortic arch and place a spherical RoI. The size and position of the RoI was manually adjusted to ensure that as much of the volume of the aortic arch as possible was captured. As the voxel dimensions of the SPECT and LDCT scans were different, the regions identified from the LDCT scan were downsampled to match the dimensions of the corresponding SPECT scan. These downsampled regions could then be used to directly mask out regions of interest from the SPECT data. The downsampled aortic arch RoI was used to isolate the SPECT voxels corresponding to blood in the aortic arch. The sum and mean of these voxels values was computed and used as a measurement of the 'background' level of activity (activity in the blood compartment). The gamma counts within the lung RoI were normalised by dividing by the mean counts in the aortic arch (representing activity in the blood pool) to generate a target-to-background ratio and therefore correct for biological clearance, as biological clearance will differ between participants.

Image analysis: Pulmonary vasculature

An AI-driven blood vessel segmentation algorithm was developed by initially manually labelling a small sample dataset using the open source 'Slicer' software (version 4.11.29219226). Labelling was performed by one clinician and one image analysis expert. The process consisted of manually 'painting' all voxels corresponding to blood vessels. The data was exported from Slicer and imported into Matlab using custom code that arranged them into a format suitable for training the neural network. A standard neural network classification model was used, with the default parameters as specified by Matlab. Balanced training sets were automatically created by randomly decimating the list of voxels classified as *not vessel* to match the number classified as *vessel*. These

balanced training sets for four subjects were then used to train and test the neural network classifier

using a leave-one-out approach.

An analysis of the effect of blood flow within the RoI was also undertaken. Unbound antibody

contained within the blood compartment flows through the RoI and does not represent the presence

of TNF- α in tissue. An automated segmentation (main text figure 3, C), using the approaches

described above, was undertaken using the LDCT scan to identify blood vessel volume within the

RoI. Vessel density was defined as blood vessel volume divided by the total RoI volume.

These values could also be applied to an equation to calculate the total normalised activity counts

within the RoI estimated to have arisen from vasculature. The expected counts within the blood

compartment were determined from the aortic arch RoI defined as the 'background.' The

normalised activity counts within the lung RoI estimated to have arisen from vasculature were

subtracted from the overall normalised activity within the lung RoI in a separate analysis.

Image analysis: Emphysema

The effect of emphysema within the RoI was analysed as it was hypothesised that antibody

deposition would be decreased in emphysematous regions due to loss of tissue density. An analysis

of the inspiratory HRCT using a density mask for percentage low attenuation area at -950

Hounsfield Units (%LAA-950) was undertaken for each participant within the COPD group to

determine degree of emphysema.

In a separate analysis, a correction was applied to determine the predicted value of median normalised SPECT activity counts if %LAA₋₉₅₀ was zero for that subject. An empirical approach using linear regression was used to correct for this. Normalised counts from study scans at the 24-hour time-point were used to inform the approach as previous studies have suggested that early time-points are more likely to reflect non-specific distribution with high vascular, liver and spleen uptake [2–4].

HRCT scans were not available for healthy volunteers due to radiation dose-reduction constraints in this group. Prior literature has provided evidence that healthy lung tissue has a low average %LAA.950 value, with population estimates between 0.2-2% [5–7]. Therefore %LAA.950 values were assumed to be zero in this group, although a further conservative analysis using %LAA.950 of 2% for all healthy volunteers was also undertaken.

Biodistribution studies

Dosimetry studies were undertaken using data from the whole-body scans. Whole body, kidney and liver regions of interest were drawn on anterior and posterior whole-body images for the 10 participants for each time point. In the case of the kidneys, activity in the right kidney was assumed to mirror that in the left kidney in order to avoid over-estimation due to organ overlay.

The cumulated activity for each region was calculated using a participant-specific conversion of counts to activity. The cumulated activity divided by the administered activity was inputted into OLINDA (Organ Level INternal Dose Assessment) [8] organ dosimetry software to calculate the

whole-body effective dose. The effective dose was scaled to the target of 370 MBq so the effective doses could be directly compared for all participants.

Immunohistochemistry studies

An immunohistochemistry study was undertaken on previously collected lung tissue samples in a heterogenous population, separate to the clinical imaging study cohort, involving patients both with and without a clinical diagnosis and spirometric evidence of COPD. Samples for immunohistochemistry studies were obtained from the TargetLung (REC number 14/SC/0186) cohort. Samples from resected lung tissue excised during surgical resection of suspected lung malignancy were collected in PBS then sectioned into volumes of approximately 1.5cm³. Samples were fixed in formalin before being embedded in paraffin wax and mounted on plastic cassettes as previously described [9]. The samples were later sectioned into 4µm slices ready for analysis.

Samples were selected from the available tissue bank based on clinical parameters of the participants within the available database to match the clinical component of the study as closely as possible. In general, the patients who had undergone lung resection had less severe COPD than those recruited to the clinical element of the imaging study, and most participants without COPD had a significant smoking history, so pragmatic selection criteria for groups were chosen. Samples from the COPD group were obtained from patients with FEV1/FVC ratio <0.7, FEV1 ≤ 55% predicted, age ≥50 and samples were selected so that mean age of the group was 65-75. Samples from the non-COPD group were obtained from patients with FEV1/FVC >0.7 and have been from

patients who were ex-smokers for ≥ 6 months or had minimal/no smoking history. Again, patients were selected with age ≥ 50 and samples were selected so that mean age of the group was 65-75.

The immunohistochemistry protocol was optimized to reduce background staining. First, sections were rehydrated through xylene substitute and graded concentrations of ethanol. To quench endogenous peroxidase activity, slides were covered with 0.5% H₂O₂ for 10 minutes then washed. Antigen retrieval was undertaken in heated sodium citrate at pH 6 for 20 minutes. After allowing to cool and washing, blocking of binding to avidin and biotin was undertaken using an Avidin/Biotin blocking kit (Vector SP-2001). Cells then underwent a permeabilization step in 0.2% Triton X-100 for 10 minutes.

Blocking buffer was applied for 30 minutes before slides were covered in 1:50 primary antibody (Abcam ab1793) suspended in blocking buffer solution. An isotype control test was also undertaken using antibody ab280974 (Abcam) as negative control, as well as anti-AA1 mast cell tryptase (Abcam ab2378) as a positive control. Slides were incubated overnight at 4°C before washing and applying secondary antibody, 1:5000 biotinylated goat anti-mouse (Abcam Ab 7067). This was incubated at 4°C for 2 hours before addition of streptavidin-horseradish peroxidase (Abcam Ab64269) for 10 minutes. Following a further wash, colour staining was undertaken with 3,3-diaminobenzidine (DAB, Abcam 64238) for up to 10 minutes. Following this, the slides were washed, counter stained with haematoxylin and dehydrated again through graded ethanols and xylene substitute.

Slides were assessed by a histopathologist for expression of TNF- α by specific tissue components in the section. Both proportion of cells (focal/diffuse) and intensity (0-3; 0 = no expression; 1 = weak expression; 2 = moderate intensity expression; 3 = strong expression) were scored.

Results supplement

Simulation of SPECT-CT activity distributions using physical and digital phantoms

Absolute quantitation of the radiopharmaceutical distribution within the torso was achieved using the Siemens xSPECT reconstruction process [10] and validated using anthropomorphic torso physical and 3-D printed radioactive phantoms.

The $^{99\text{m}}$ Tc activity concentration, mean standardised uptake value (SUV_{mean}) and the recovery coefficient for all regions, as well as the recovery curve for the spheres are shown in *figure S1* (parts A and C). The phantom study results showed that xSPECT acquisition and reconstruction allows detection of small sized activity distribution down to 1ml within the lung parenchyma at contrast and the signal to noise levels anticipated, verifying the suitability of xSPECT data for use within the lung imaging protocol and to inform further analysis (figure S1, part C).

With regards to activity quantification, quantitative analysis of activity recovery highlighted that xSPECT-derived estimates of activity concentrations are reasonable for volumes larger than around 4ml (figure S1, part A). As would be expected for a clinical SPECT-CT system, measurement uncertainty [11], due to reasons such as partial volume effect [12], results in

significant reduction of accuracy in estimating activity concentration for smaller volumes. These results outline the limitations of our selected quantitative imaging protocol and informed the design of post imaging analysis. More complex phantom distributions were investigated using a radioactive InkJet printing technique. Images obtained using the SPECT-CT protocol are shown in *figure S1*, **D** and **E**.

Labelling of anti-TNF-α with ^{99m}Tc

Mean radiochemical purity was 97.5% (range 91-99%, SD 2.51) and maintained at >95% for 9 of the 10 infusions using this approach. Sterility studies confirmed sterility for each radiolabelled product used in the study.

Testing of vessel segmentation tool

To ensure that the AI segmentation tool developed for analysis of vessel density was accurately selecting blood vessels, AI segmentation was compared to manual segmentation data using a leave-one-out training approach. This analysis revealed a sensitivity of 91.28% and specificity of 92.75% of the AI segmentation tool.

Calculation of vessel density

Mean vessel density in the healthy group was 0.132 +/- 0.023 and was 0.088 +/- 0.018 in the COPD group. The differences between groups were statistically significant (p=0.016). The mean of vessel density values across the 6- and 24-hour scans was used as there were small variations in vessel

density between these time-points due to the free-breathing nature of scans (maximum intrasubject variation in vessel density between the 6- and 24-hour scan time-points was 0.022).

Adjustment for heterogeneity of tissue density – conservative analysis

In addition to the data presented in the main text, a further conservative analysis assuming %LAA. 950 in healthy subjects of 2% did not reverse the trend of higher corrected counts in the COPD group. At the 6-hour time-point corrected counts were (mean +/- SD) 0.192 +/- 0.027 in the healthy group and 0.225 +/- 0.038 in the COPD group. At the 24-hour time point this was 0.260 +/- 0.089 in the healthy group and 0.285 +/- 0.017 in the COPD group (*supplementary figure S2*). Differences between groups were not statistically significant.

Multiple regression model

A multiple regression analysis was undertaken to determine the combined effects of both emphysema and vessel density on C_n . The results indicate a good fit of the model at the 24-hour time-point (F(3,6)=6.959, p=.022, R²=0.777). When adjusting for both %LAA₋₉₅₀ and vessel density, C_n were shown to be higher for patients in the COPD group than healthy volunteers (β =.066) but this result did not reach statistical significance (p=.407, 95% CI [-.116, .249]) as was also the case for %LAA₋₉₅₀ (β =-.002, p=.412, 95% CI [-.009, .004]). However, vessel density was found to be a significant predictor of C_n (β =2.431, p=.044, 95% CI [.088, 4.774]). There was also good fit of the model at the 6-hour time-point (F(3,6)=16.793, p=.003, R²=.894) but there were no individual significant predictors from each of participant group (β =-.048, p=.183, 95% CI [-1.26,

0.030]), %LAA₋₉₅₀ (β= -.001, p=.357, 95% CI [-.004, .002]) and vessel density (β=.384, p=.383, 95% CI [-.614, 1.383]).

Analysis of additional phenotyping data

Bivariate correlations between median normalised counts and phenotyping data are shown in *table* SI. A number of the correlations seen correspond to the differences between COPD and healthy participant groups, such as higher FEV₁ and lower symptom scores in the healthy group. Analysis by group is likely to be of greater utility and is included in the main text.

Smoking status was collected from participants and difference in median normalised counts according to smoking status is shown in *figure S3*. There was a statistically significant difference between groups at the 6-hour time point (p=.002 one way ANOVA), but difference was between the never smoker group and the remaining two groups (never smoker – ex-smoker p=.004; never smoker – current smoker p=.004; comparison by Tukey's Honestly Significant Difference). All never smokers were in the healthy group, therefore this reflects the difference between the healthy and COPD group. There were no statistically significant differences at the 24-hour time point, or when analysing the difference between 6-24 hour time point scans.

Blood and sputum TNF-a

Mean plasma TNF-α concentration (+/- SD) for the healthy control group was 21.98 pg/ml +/- 31.39 and for the COPD group was 0.61 pg/ml +/- 0.3712. Mean serum concentration in the healthy control group was 76.43 pg/ml +/- 73.13 and in the COPD group was 6.09 pg/ml +/- 4.93 (*figure S4*). The differences between groups were not statistically significant.

Sputum sampling by induced sputum was only possible for two participants in the cohort due to participants either being unable to undertake the procedure due to safety/tolerability, or due to COVID-19 restrictions that were in place at the time of the study.

Aortic arch counts

Mean counts +/- SD within the aortic arch at the 6hr time-point were 26.50 s⁻¹ +/- 5.86 for the healthy group and 31.18 s^{-1} +/- 8.00 for the COPD group (*figure S5*). At the 24-hr time point, mean counts were 5.08 s^{-1} +/- $2.03 \text{ for the healthy group and } 5.74 \text{ s}^{-1}$ +/- 1.60 for the COPD group.

Biodistribution of anti-TNF-α antibody

As part of establishing the safety profile of ^{99m}Tc-infliximab and regulatory sign-off for the study, radiation dose estimates prior to study start were calculated based on data for ^{99m}Tc-labelled monoclonal antibodies using ICRP 106 [13]. The whole-body effective dose for an average adult male was calculated to be 3.63 mSv for 370 MBq of ^{99m}Tc-labelled monoclonal antibodies. An additional calculation using data from a mouse model [2] provided a further estimate for whole-body effective dose of 1.08mSv.

Whole body images obtained during the clinical component of our study underwent dosimetry analysis. Mean effective dose (+/-SD) from the ^{99m}Tc-infliximab tracer for participants in the healthy group was 1.69 mSv +/- 0.04 and mean effective dose for participants in the COPD group was 1.74 mSv +/- 0.07. When scaled to 370 MBq, the calculated whole-body effective doses were well within the predicted effective dose and within a range of 0.18 mSv for all participants (*table*

S2). The absorbed radiation doses to potential organs at radiological risk (liver and kidneys) were well within safe margins.

Safety

The dose of anti-TNF- α infused was <1/1000th of the therapeutic dose and no pharmacological effects are anticipated at this dose. No safety issues arose during the study and no pharmacological effects were observed. A review of safety data with the external safety assessor occurred after the first participant (healthy group) and second participant (COPD group) had undergone study procedures. For each participant following this, a safety report was sent to the external safety assessor after each participant had completed the study. No serious adverse events (SAEs) arose during the study.

Three participants suffered adverse events during the clinical phase of the study unrelated to study procedures (exacerbation of COPD, diarrhoea and vomiting, and exercise-induced musculoskeletal pain). Two participants suffered a short episode of breathlessness after lying flat for the scan, which was consistent with their known COPD. However, the procedure was safe and, overall, well tolerated.

Tissue distribution of TNF-α by immunohistochemistry

In the separately collected samples, TNF- α expression was highest in alveolar macrophages and moderately intense expression was seen in airway and alveolar epithelial cells, as well as acellular stroma (*figure S6*). Weak intensity expression was detected in lymphocytes and vascular endothelium, occasional stromal cells and no expression was seen in smooth muscle cells. The

immunohistochemistry results support the hypothesis that the development of emphysema reduces the volume of tissue in which TNF- α is expressed, with both airway and alveolar epithelium being lost in the development of emphysema. Given that the immunohistochemistry control group was a heterogenous group, including several patients having a significant smoking history (*figure S6*, G), and the majority of patients from both groups having lung resection for lung cancer, between group comparisons have not been made due to these shared factors being assessed as likely to contribute to TNF- α expression [14, 15].

Supplementary figures and tables

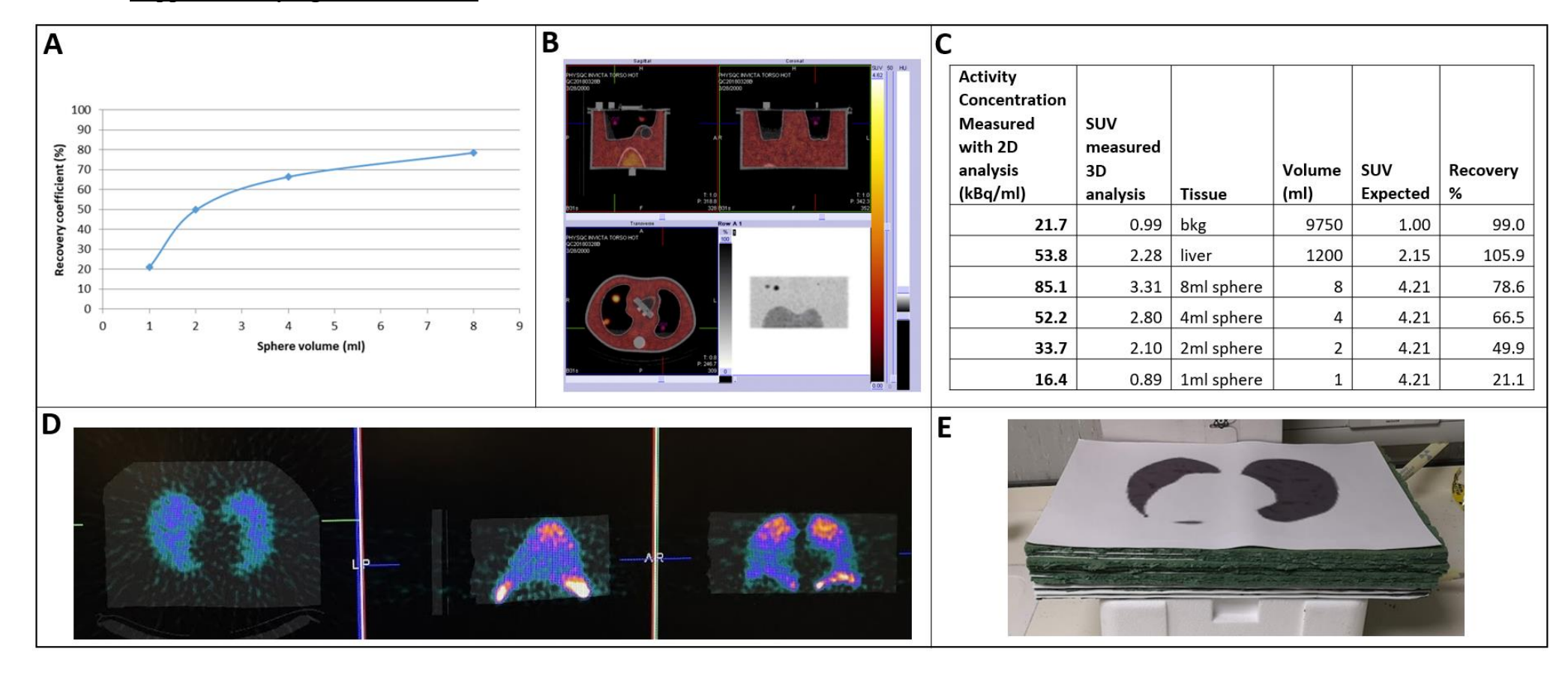


Fig S1 Phantom study. Recovery coefficients for 4 spheres filled with Tc-99m ranging from 1 to 8ml are shown in the graph in **A**. Fused SPECT-CT images of the anthropomorphic phantom are shown in **B**, and the table in **C** shows the measured activity concentration, SUV, volume and recovery coefficient for the 4 fillable spheres, liver and background regions. SPECT-CT reconstruction of the printed phantom is shown in **D**. The printed phantom was formed by applying the required radioactive distribution to a sequence of paper sheets and these were supported by a foam scaffold (**E**).

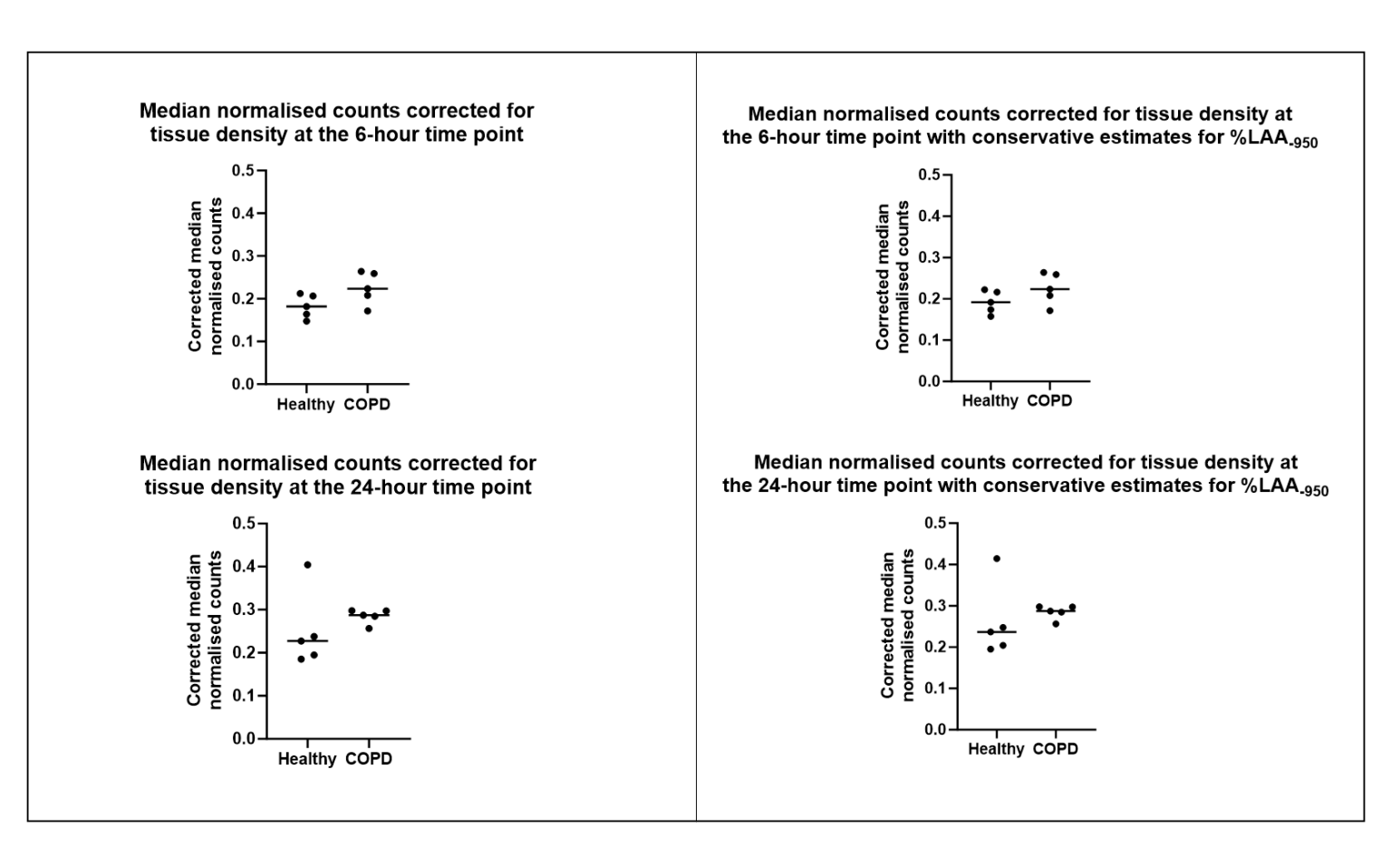


Fig S2 Corrections for tissue density. Median normalised counts after correcting for the effect of tissue density on anti-TNF- α signal (A) using the regression line derived from the study data. A further conservative analysis was undertaken (B), assuming all healthy volunteers to have %LAA.950 at the upper end of estimates in the literature of 2%. Both analyses revealed higher anti-TNF- α signal in the COPD group after correction, but this difference was not statistically significant

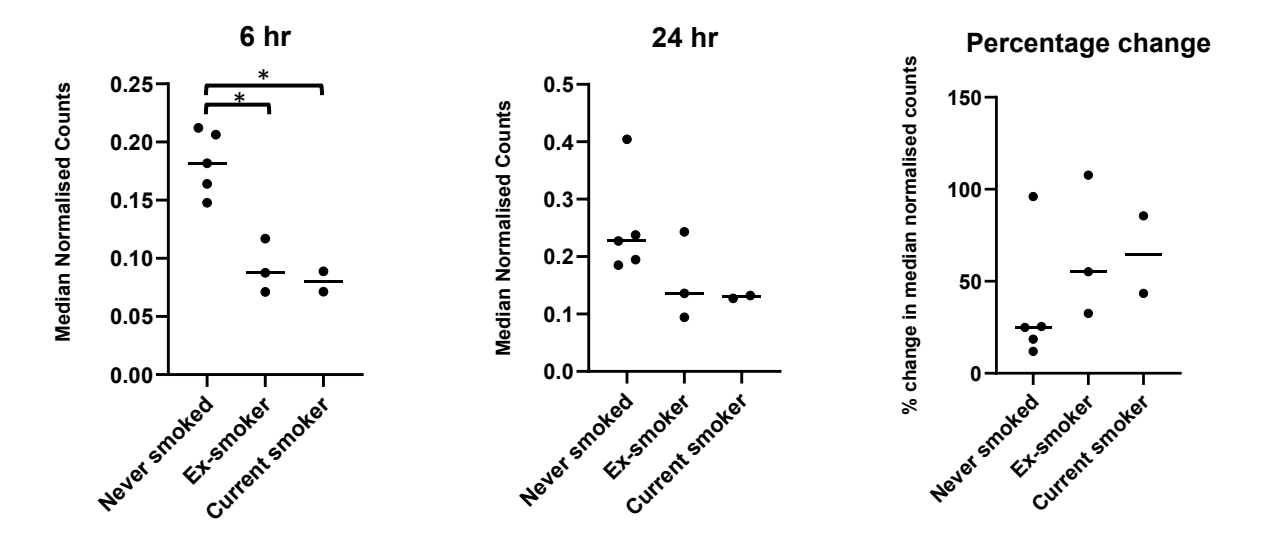


Fig S3 Differences between smoking groups. There were significant differences only between the healthy group participants (never smoked) and participants in each of the other smoking groups at the 6-hour time point. Significance to the p < 0.01 level indicated by * (one way ANOVA with post-hoc adjustment by Tukey's HSD)

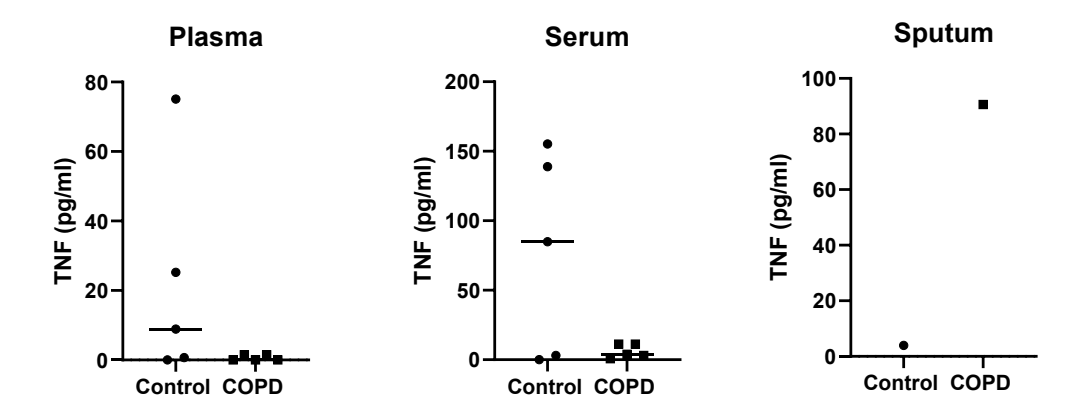


Fig S4 Blood and sputum TNF-α. Mean plasma concentration (+/- SD) for the healthy control group was 21.98 pg/ml +/- 31.39 and for the COPD group was 0.61 pg/ml +/- 0.3712. Mean serum concentration in the healthy control group was 76.43 pg/ml +/- 73.13 and in the COPD group was 6.09 pg/ml +/- 4.93. Differences in plasma and serum TNF-α concentrations between groups were not statistically significant. Due to restrictions on sputum sampling at the time of the study, and some participants being unable to undergo sputum induction, n=1 in each group for sputum samples therefore this data is not analysed.

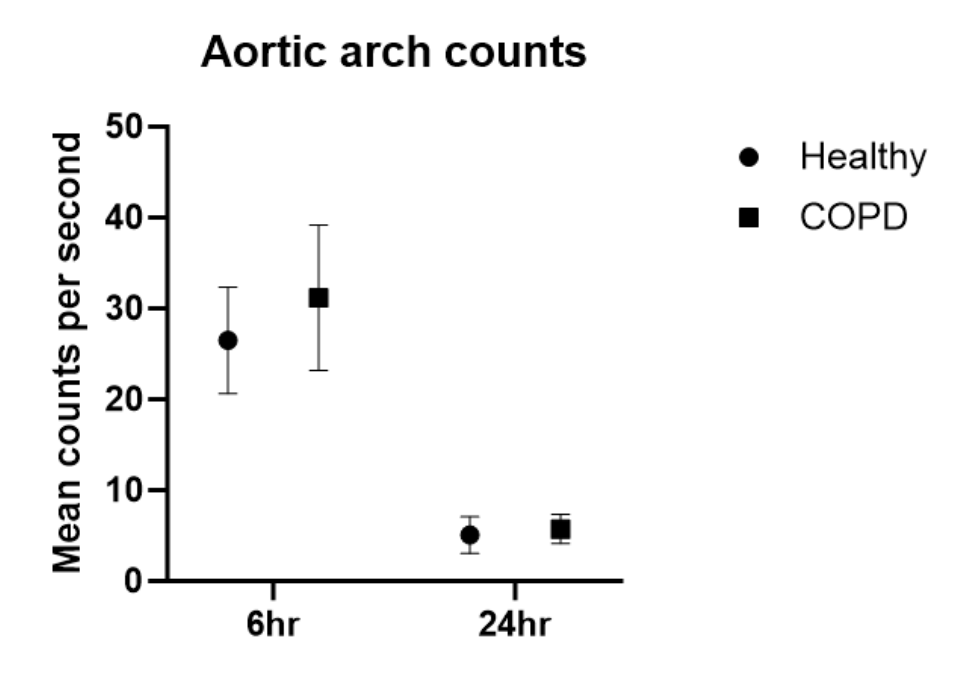


Fig S5 Aortic arch counts. Mean SPECT voxel counts within the region of interest defined as 'background' during the normalisation process. The region of interest was defined within the vasculature at the aortic arch. Counts per second are shown at each time point for each group

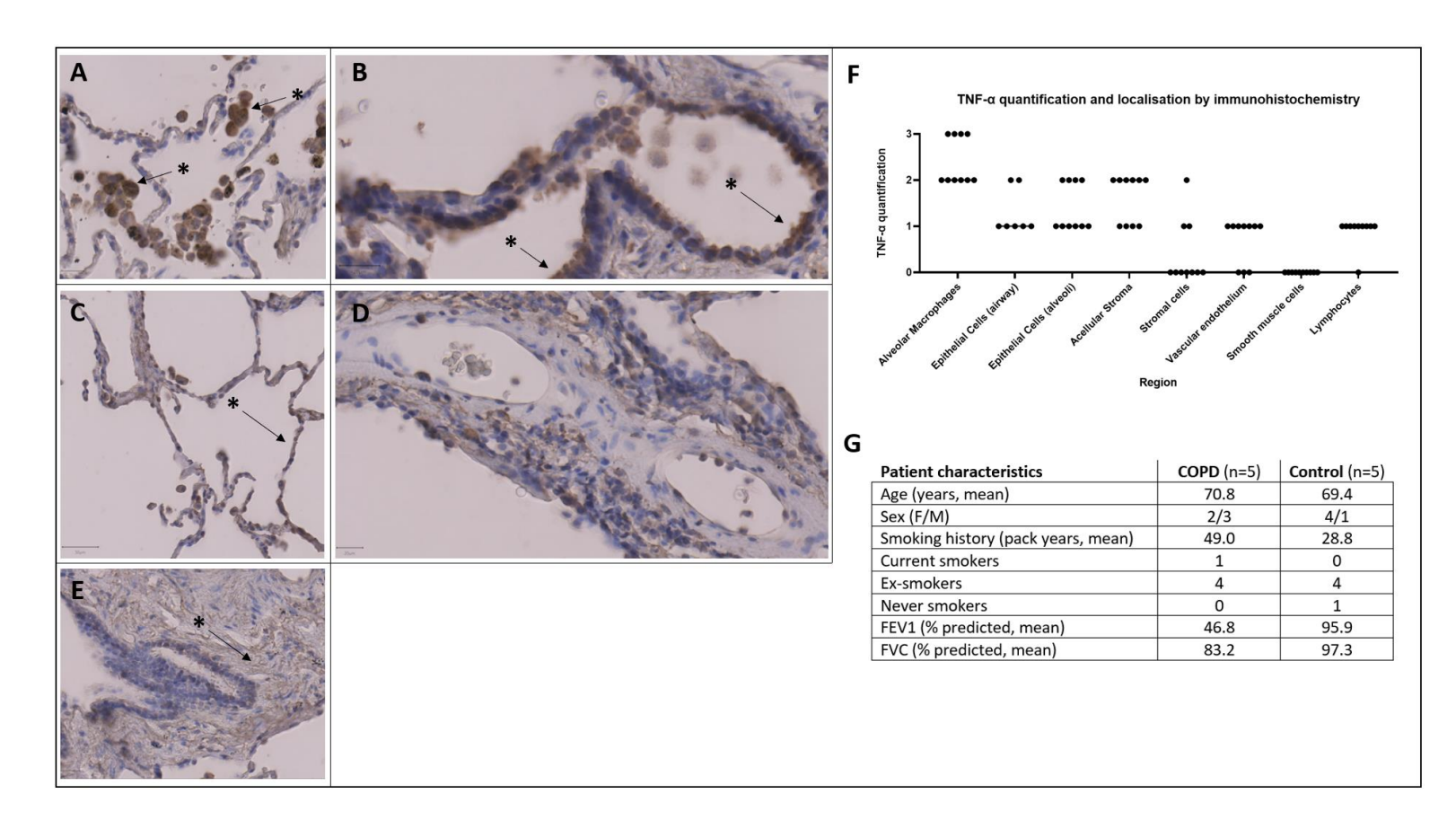


Fig S6 Immunohistochemistry for TNF-α undertaken in tissue samples from patients with or without COPD. Light microscopy images are shown in A-E, with examples of areas of positive expression indicated with an asterisk (*). There was strong TNF-α expression in macrophages (A) and airway epithelium (healthy subject shown in B). Expression by alveolar epithelium in COPD is shown in C, and absence of expression by vascular endothelium of a subject with COPD is shown in D. Expression within acellular stroma is shown in a specimen from a patient with COPD in E. A graph of quantification of expression within specific regions of tissue (F; 0 = no expression; 1 = weak expression; 2 = moderate intensity expression; 3 = strong expression) and a table of participant characteristics within each group (G) are provided.

	FEV1 %	FVC %	FEV1/FVC	TLCO %	KCO %	RV %	RV/TLC	Fat Free Mass (%)	CAT score	mMRC score
Median normalised counts – 6hr time point	.857*	.857*	929**	.845**	.733*	867**	879**	190	634*	888**
	p=0.014	p=0.014	p=0.003	p=0.002	p=0.016	p=0.001	p=0.001	p = 0.651	p=0.049	p=0.001
Median normalised counts – 24hr time point	.857*	.857*	929**	.596	.564	782**	709*	071	443	645*
	p=0.014	p=0.014	p=0.003	p=0.069	p=0.090	p=0.008	p=0.022	p=0.867	p=0.200	p=0.044
Percentage change in median normalised counts	821*	821*	750	571	503	.248	.406	.571	.603	.480
	p=0.023	p=0.023	p=0.052	p=0.084	p=0.138	p=0.489	p=0.244	p=0.139	p=0.065	p=0.160
Median normalised counts corrected for tissue density – 6hr time point	536	.536	500	675*	648*	.491	.552	.071	.677*	.612
	p=0.215	p=0.215	p=0.253	p=0.032	p=0.043	p=0.150	p=0.098	p=0.867	p=0.032	p=0.060
Median normalised counts corrected for tissue density – 24hr time point	714	714	643	571	503	.055	.236	.571	.652*	.428
	p=0.071	p=0.071	p=0.119	p=0.084	p=0.138	p=0.881	p=0.511	p=0.139	p=0.041	p=0.218

Table S1. Correlations between measures for SPECT signal and lung function results or questionnaire scores. Values presented are by Spearman's correlation coefficient. Correlations for FEV1 %, FVC % and FEV1/FVC are based on pre-bronchodilator values. FEV1 %, forced expiratory volume in 1 second percent predicted; FVC %, forced vital capacity percent predicted; FEV1/FVC, ratio of FEV1 to FVC (Tiffeneau index); TLCO %, transfer factor of the lung for carbon monoxide percent predicted; KCO %, carbon monoxide transfer coefficient percent predicted; RV %, residual volume percent predicted; CAT, COPD assessment tool; mMRC, modified Medical Research Council dyspnoea scale. * p<0.05; **p<0.001

	n	Minimum	Maximum	Mean	Std. Deviation
Effective dose – Healthy participant group	5	1.63	1.73	1.69	0.04
Effective dose – COPD group	5	1.65	1.81	1.74	0.07

Table S2. Summary of absorbed radiation doses from 99mTc-anti-TNF tracer injection. Dosimetry calculations were undertaken using anterior and posterior whole-body images obtained at each scan time-point. The effective dose was scaled to the target of 370 MBq so the effective doses could be directly compared for all participants.

Supplementary references

- 1 Mather SJ, Ellison D. Reduction-mediated technetium-99m labeling of monoclonal antibodies. *Journal of Nuclear Medicine* 1990; 31: 692–697.
- D'Alessandria C, Malviya G, Viscido A, et al. Use of a 99mTc labeled anti-TNFa monoclonal antibody in Crohn's disease: in vitro and in vivo studies. The Quarterly Journal of Nuclear Medicine and Molecular Imaging 2007; : 334–342.
- Conti F, Malviya G, Ceccarelli F, *et al.* Role of scintigraphy with 99mTc-infliximab in predicting the response of intraarticular infliximab treatment in patients with refractory monoarthritis. *Eur J Nucl Med Mol Imaging* 2012; 39: 1339–1347.
- 4 Vis R, Malviya G, Signore A, *et al.* 99mTc-anti-TNF-α antibody for the imaging of disease activity in pulmonary sarcoidosis. *European Respiratory Journal* [Internet] 2016; 47: 1198–1207. Available from: http://dx.doi.org/10.1183/13993003.01352-2015.
- Hoffman EA, Ahmed FS, Baumhauer H, et al. Variation in the percent of emphysema-like lung in a healthy, nonsmoking multiethnic sample. The MESA Lung Study. *Ann Am Thorac Soc* 2014; 11: 951–955.
- Zach JA, Newell JD, Schroeder J, *et al.* Quantitative computed tomography of the lungs and airways in healthy nonsmoking adults. *Invest Radiol* 2012; 47: 596–602.
- 7 Cheng T, Li Y, Pang S, *et al.* Normal lung attenuation distribution and lung volume on computed tomography in a Chinese population. *International Journal of COPD* 2019; 14: 1657–1668.
- Stabin MG, Sparks RB, Crowe E. OLINDA/EXM: The second-generation personal computer software for internal dose assessment in nuclear medicine. *Journal of Nuclear Medicine* 2005; 46: 1023–1027.
- 9 Lawson MJ, Katsamenis OL, Chatelet D, et al. Immunofluorescence-guided segmentation of three-dimensional features in micro-computed tomography datasets of human lung tissue. R Soc Open Sci 2021; 8.
- Armstrong IS, Hoffmann SA. Activity concentration measurements using a conjugate gradient (Siemens xSPECT) reconstruction algorithm in SPECT/CT. *Nucl Med Commun* 2016; 37: 1212–1217.

- Gear JI, Cox MG, Gustafsson J, *et al.* EANM practical guidance on uncertainty analysis for molecular radiotherapy absorbed dose calculations. *Eur J Nucl Med Mol Imaging* Springer Berlin Heidelberg; 2018; 45: 2456–2474.
- Rousset OG, Ma Y, Evans AC. Correction for partial volume effects in PET: principle and validation. *J Nucl Med* [Internet] 1998; 39: 904–911. Available from: http://www.ncbi.nlm.nih.gov/pubmed/9591599.
- Valentin J. Radiation dose to patients from radiopharmaceuticals. Addendum 3 to ICRP Publication 53. ICRP Publication 106. Approved by the Commission in October 2007. *Ann ICRP* [Internet] 2008; 38: 1–197. Available from: http://journals.sagepub.com/doi/10.1016/j.icrp.2008.08.003.
- 14 Matanić D, Beg-Zec Z, Stojanović D, *et al.* Cytokines in patients with lung cancer. *Scand J Immunol* 2003; 57: 173–178.
- 15 Balkwill F. Tumor necrosis factor or tumor promoting factor? Cytokine Growth Factor Rev 2002.